Mapping the pathogenesis of immune-mediated aplastic anemia: filling the gaps

Pool, E.S.

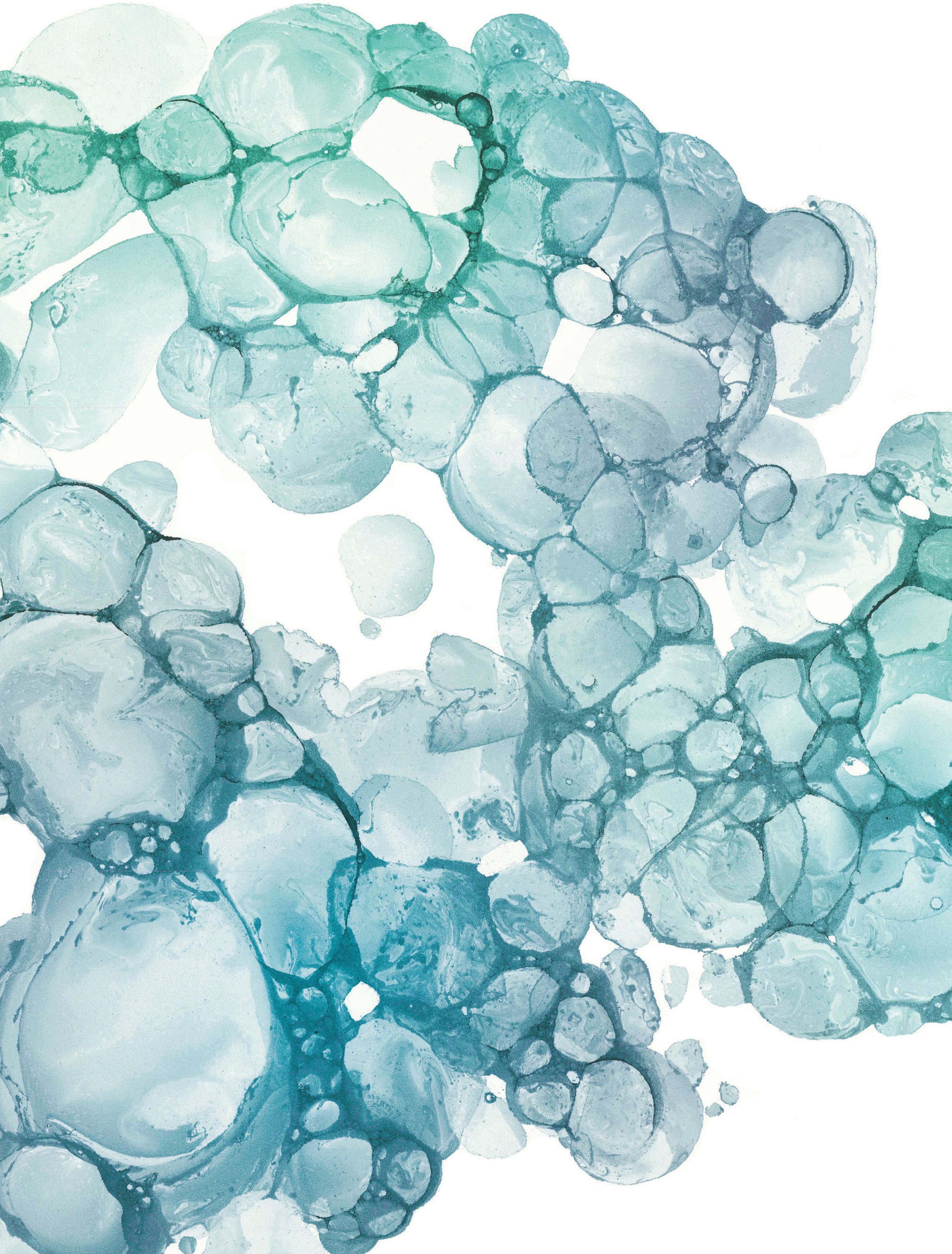

2

Mass cytometric analysis unveils a disease-specific immune cell network in the bone marrow in acquired aplastic anemia

Emma S. Pool[1], Yvonne Kooy-Winkelaar[2], Vincent van Unen[2,3], J.H. Frederik Falkenburg[1], Frits Koning[2], Mirjam H.M. Heemskerk[1] and Jennifer M-L. Tjon[1]

[1] Department of Hematology, Leiden University Medical Center, Leiden, The Netherlands
[2] Department of Immunology, Leiden University Medical Center, Leiden, The Netherlands
[3] Institute for Immunity, Transplantation and Infection, Stanford University, California, USA

Frontiers in Immunology (2023)
DOI: 10.3389/fimmu.2023.1274116

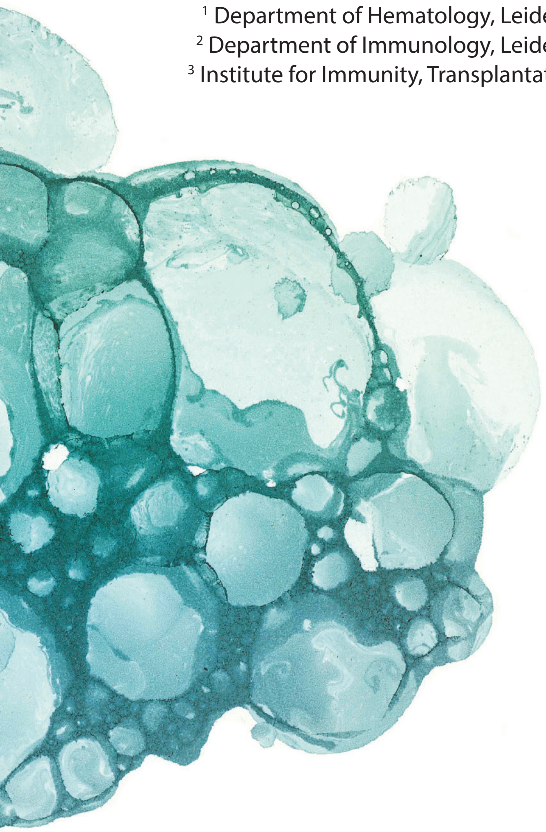

Key points

- Broad immunophenotyping by mass cytometry provides a detailed overview of the immune landscape in the bone marrow in aplastic anemia
- A disease-specific immune cell network that shows a trend toward normalization after successful treatment was identified.

Visual abstract

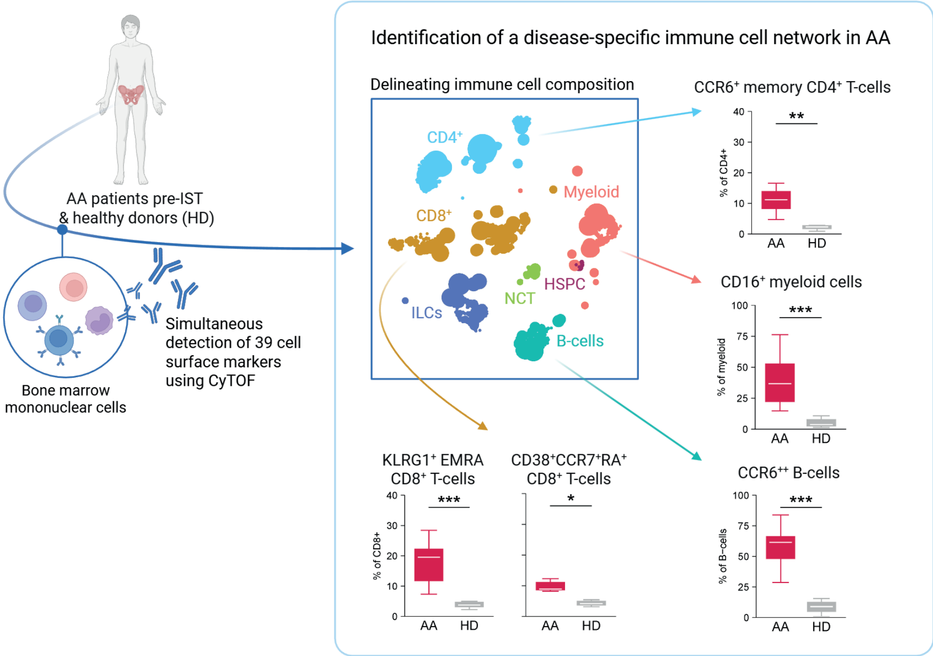

Abstract

Idiopathic acquired aplastic anemia (AA) is considered an immune-mediated syndrome of bone marrow failure since approximately 70% of patients respond to immunosuppressive therapy (IST) consisting of a course of anti-thymocyte globulin (ATG) followed by long-term use of ciclosporin. However, the immune response that underlies the pathogenesis of AA remains poorly understood. In this study, we applied high-dimensional mass cytometry on bone marrow aspirates of AA patients pre-ATG, AA patients post-ATG and healthy donors to decipher which immune cells may be implicated in the pathogenesis of AA. We show that the bone marrow of AA patients features an immune cell composition distinct from healthy donors, with significant differences in the myeloid, B-cell, $CD4^+$ and $CD8^+$ T-cell lineages. Specifically, we discovered that AA pre-ATG is characterized by a disease-specific immune cell network with high frequencies of $CD16^+$ myeloid cells, $CCR6^{++}$ B-cells, Th17-like $CCR6^+$ memory $CD4^+$ T-cells, $CD45RA^+CCR7^+CD38^+$ $CD8^+$ T-cells and $KLRG1^+$ terminally differentiated effector memory (EMRA) $CD8^+$ T-cells, compatible with a state of chronic inflammation. Successful treatment with IST strongly reduced the levels of $CD16^+$ myeloid cells and showed a trend towards normalization of the frequencies of $CCR6^{++}$ B-cells, $CCR6^+$ memory $CD4^+$ T-cells and $KLRG1^+$ EMRA $CD8^+$ T-cells. Altogether, our study provides a unique overview of the immune landscape in the bone marrow in AA at a single-cell level and proposes CCR6 as a potential new therapeutic target in AA.

Introduction

Idiopathic acquired aplastic anemia (AA) is characterized by bone marrow hypocellularity due to a profound decrease in hematopoiesis resulting in pancytopenia[1]. Symptoms of AA relate to the severity of pancytopenia and severe cases of AA are potentially fatal, mainly due to bleeding and infectious complications.

Two effective treatments can result in recovery of hematopoiesis: allogeneic hematopoietic stem cell transplantation (allo-HSCT) and immunosuppressive therapy (IST)[1-3]. First-line allo-HSCT leads to rapid recovery of hematopoiesis but has a risk of graft-versus-host disease and transplant-related mortality and is therefore only recommended for patients under the age of 40 with an HLA-identical sibling donor[4]. Accordingly, IST is the preferred first-line treatment in most AA patients.

Standard IST for AA combines ciclosporin and anti-thymocyte globulin (ATG), a polyclonal IgG antibody preparation that is manufactured by immunizing animals with human thymocytes. In the setting of AA both rabbit-derived ATG (rATG) and horse-derived ATG (hATG) have been applied. However, hATG is preferred since hematological response to hATG is superior to rATG[5,6]. In patients responsive to IST, peripheral blood counts gradually recover within several months. Therefore, international guidelines recommend response evaluation 3-6 months after the start of IST. Consequently, non-responding patients are identified after months of prolonged cytopenia and remain at risk for bleeding and infectious complications. One-third of patients fail to recover sufficiently after IST[6]. At present, it is not possible to predict at diagnosis which patients will respond to IST.

Better understanding of the pathogenesis of AA could aid in timely identifying patients that are less likely to respond to IST. Bone marrow recovery after IST strongly implies an immune-mediated pathogenesis in AA. Because ATG results in lymphocyte depletion and effector T-cells are expanded in AA[7], a widely accepted view is that hematopoietic stem and progenitor cells (HSPCs) in the bone marrow are targeted by autoreactive T-cells. However, if AA would only be mediated by T-cells, it is surprising that hATG is superior to rATG, since hATG is less potent at depleting lymphocytes[5,6]. Therefore, we include the possibility that the therapeutic effect of hATG goes beyond T-cell depletion and involves an effect on other immune cell populations as well.

Previous research extensively investigated immune cells in peripheral blood in AA and suggested a role for T-cell[8,9] and B-cell[10] subpopulations in its pathogenesis. However, a detailed overview of the immune landscape at the site of HSPC destruction, the bone marrow, is lacking. The few studies that reported T-cell abnormalities in the bone marrow could not provide a full overview of the immune cell composition due to limitations in the size of flow cytometry antibody panels. In recent years, high-dimensional discovery tools like single-cell RNA sequencing (scRNA-seq) or mass cytometry offered new possibilities to study the immune system in tissues[11]. Mass cytometry, in contrast to scRNA-seq, quantifies protein expression levels on single-cells and therefore allows for the exploration of both common and rarer immune subpopulations. In the present study, we applied mass cytometry on bone marrow aspirates of AA patients. This enabled us to reveal a considerable shift in the immune cell composition in bone marrow from AA patients and to identify a disease-specific immune cell network. Our study contributes to our understanding of AA as an immune-mediated form of bone marrow failure and shows that not only T-cells, but also myeloid cells and B-cells are likely involved in its pathogenesis.

Methods

Patients and samples

Bone marrow aspirates and peripheral blood samples were collected from 7 adult AA patients at diagnosis (pre-ATG; AA^{PRE}) and 7 age- and sex-matched healthy donors (HDs). In addition, bone marrow aspirates from 3 of 7 AA patients were collected six months after the start of first-line IST (post-ATG; AA^{POST}), which consisted of 4 days of 40 mg/kg ATGAM® (hATG; Pfizer) and 5 mg/kg/day ciclosporin for at least six months. Bone marrow and peripheral blood collection were performed after given informed consent in accordance with the Declaration of Helsinki. Clinical characteristics of patients and HDs are outlined in Table 1. All patients were treatment-naïve at diagnosis, had an indication for treatment, did not have an additional underlying disease and were diagnosed and treated according to Dutch guidelines[3]. Patients under the age of 40 were screened for Fanconi anemia to rule out a congenital form of bone marrow failure. One patient was classified as non-severe AA (NSAA), two patients as severe AA (SAA) and four patients as very severe AA (VSAA), defined as described in international guidelines[2]. Complete response to IST was defined as complete normalization of peripheral blood counts. Partial response was defined as transfusion independence and a neutrophil count of at least $0.5 \cdot 10^9$ neutrophils/L. This study was approved by the Medical Ethical Committee of the Leiden University Medical Center (protocol number B20.037).

Table 1. Characteristics of patients and response to IST.

Characteristic	AA^PRE	AA^POST	HD
Patients (n)	7	3	7
Age (median, range in years)	31 (23-42)	28 (27-40)	31 (24-44)
Sex (n, M:F)	4:3	2:1	4:3
Severity of disease (n)			
Non-severe AA	1	0	NA
Severe AA	2	1	NA
Very severe AA	4	2	NA

AA indicates aplastic anemia; F: female; IST: immunosuppressive therapy; M: male; NA: not applicable.

Mass cytometry antibody staining, data acquisition and data analysis

Bone marrow mononuclear cells (BMMCs) or peripheral blood mononuclear cells (PBMCs) were isolated from bone marrow aspirates or peripheral blood, stained with a panel of 39 validated[12-14] metal-isotope tagged antibodies and measured as described in Supplemental Methods. For each acquired mass cytometry data file, single, live $CD45^+$ cells were gated in FlowJo version 10.7.1 (BD Biosciences) as shown in Figure S1. A median of $0.5 \cdot 10^6$ (range 0.4-$0.9 \cdot 10^6$) cells was gated for each AA^{PRE} sample. For every HD or AA^{POST} sample, a median of $0.5 \cdot 10^6$ (range 0.3-$0.9 \cdot 10^6$) or $0.3 \cdot 10^6$ (range 0.3-$0.6 \cdot 10^6$) cells was gated respectively.

The single, live $CD45^+$ cells were studied using two analyses. In the first analysis, BMMC samples from all AA^{PRE} and HDs were studied. $7.7 \cdot 10^6$ single, live $CD45^+$ cells were sample-tagged, hyperbolic arcsinh transformed with a cofactor of 5 and imported into Cytosplore[15] for dimensionality reduction. A five-level hierarchical stochastic neighbor embedding (HSNE) analysis was performed with default perplexity and iterations (30 and 1000, respectively; see Figure S2 for outline of HSNE analysis pipeline). Three of 39 markers in the mass cytometry panel (HLA-DR, CD5 and KLRG1) were not used in the HSNE clustering analysis due to small variations in marker distribution between experiments (data not shown). Major immune lineages were identified at the overview level of the HSNE analysis and were defined as: $CD4^+CD3^+CD7^+$ $CD4^+$ T-cells, $CD8a/b^+CD3^+CD7^+$ $CD8^+$ T-cells, $CD7^-CD20/IgM^+$ B-cells, $CD3^+CD7^+TCRgd^+$ non-conventional T-cells (NCTs), $CD3^-CD7^+$ innate lymphoid cells (ILCs) including NK-cells and Lin^-cKit^+ HSPCs. All remaining cells were considered myeloid cells. Subsequently, each major immune lineage was selected for detailed analysis at the data level of the HSNE analysis using t-distributed stochastic neighbor embedding (tSNE) analyses with up to $0.5 \cdot 10^6$ landmarks. Clusters with distinct surface marker expression were identified within each major immune lineage by Gaussian mean shift (GMS) clustering at the data level. Each cluster consisted of at least 1000 cells (Figure S2).

In the second analysis, paired BMMC samples from 3 AA^{PRE} and AA^{POST} were analyzed using a comparable approach, for detailed description, see Supplemental Methods.

After clustering in both analyses, .fcs files of major immune lineages and clusters were exported from Cytosplore and loaded into R version 4.0.5 for data visualization and analysis. Cytofast[16] was used to generate heatmaps and to compare lineage or cluster frequencies between groups. Principal component analyses (PCA) and a Spearman's rank correlation analysis were performed using the packages factoextra version 1.0.7[17] and corrplot version 0.92[18], respectively.

Statistical analysis

Mann-Whitney *U* tests performed in R version 4.0.5 were used to compare immune cell frequencies between two groups. *P*-values ≤ 0.05 were considered statistically significant. Since this was an exploratory study, no adjustments for multiple testing were applied. $^{*}P \leq 0.05$; $^{**}P \leq 0.01$; $^{***}P \leq 0.001$.

Results

The immune cell composition in bone marrow of AA patients pre-ATG is distinct from healthy donors

First, we studied the immune cell composition in the bone marrow of the 7 AA^{PRE} and 7 age- and sex-matched HDs. A five-level HSNE analysis was performed to visualize all $7.7{\cdot}10^6$ $CD45^+$ cells (median $0.5{\cdot}10^6$ $CD45^+$ cells per sample). At the overview level of the HSNE analysis, all major immune lineages and HSPCs could be identified by clustering based on lineage markers and cKit (Figure 1A). All AA^{PRE} and HD samples were homogeneously distributed per group over the HSNE analysis (Figure S3). Visualization of the AA^{PRE} and HDs in the overview level already revealed clear differences in the immune cell composition.

An unsupervised PCA confirmed a clear separation in the immune cell composition of AA^{PRE} and HDs (Figure 1B). Next, the immune cell composition was studied in further detail at the major immune lineage level. Since we aimed to uncover how the immune cell composition differs in bone marrow from AA^{PRE} and HDs and total cell counts are decreased in the bone marrow in AA, we studied relative cell frequencies instead of absolute cell counts. Major immune lineage frequencies of $CD45^+$ cells were determined (Figure 1C). HSPCs could not be distinguished enough at this level of the HSNE analysis and were therefore merged with myeloid cells. In agreement with disease characteristics, myeloid cells were scarce in AA^{PRE} compared to HDs (median 0.6% *versus* 33% of $CD45^+$ cells). B-cells were also reduced in AA^{PRE} compared to HDs (median 9% *versus* 16% of $CD45^+$ cells). In contrast, $CD4^+$ and $CD8^+$ T-cells were increased in AA^{PRE} compared to HDs, which could be due to the relative decrease in myeloid and B-cells. Finally, non-conventional T-cell (NCT) and innate lymphoid cell (ILC) frequencies did not significantly differ between AA^{PRE} and HDs.

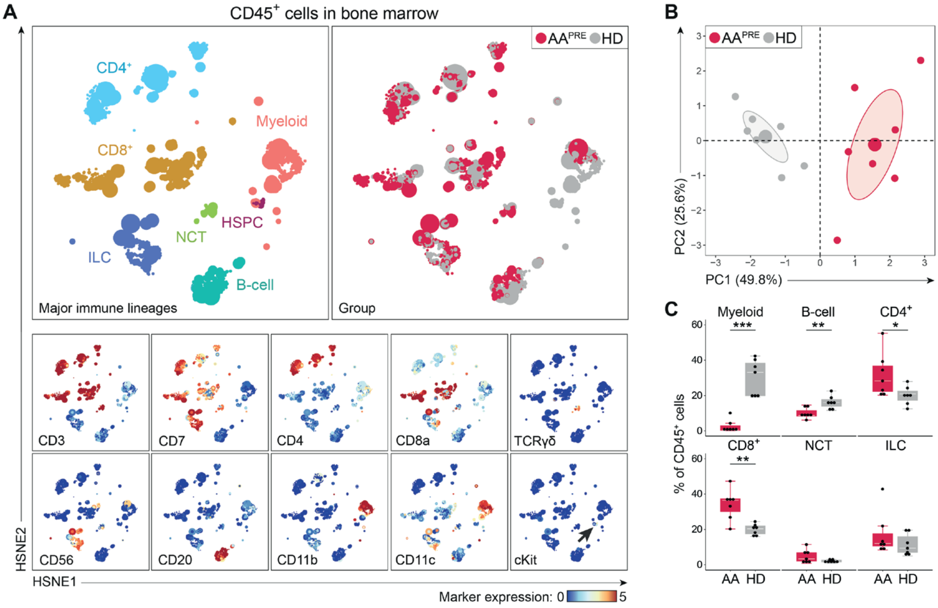

Figure 1. Major immune lineages in bone marrow in AA pre-ATG and HD. Colors indicate major immune lineages (HSPCs, myeloid cells, B-cells, $CD4^+$ T-cells, $CD8^+$ T-cells, NCT-cells and ILCs), groups (AA^{PRE} in red and HDs in gray) or median ArcSinh-transformed marker expression values. (A) Major immune lineages in bone marrow of 7 AA^{PRE} and 7 HDs, visualized at the overview level of a five-level HSNE analysis. $7.8 \cdot 10^3$ HSNE landmarks represented all $7.7 \cdot 10^6$ $CD45^+$ cells in the analysis. The size of each landmark reflects the number of cells represented by the landmark. $cKit^+$ cells are indicated by an arrow. Major immune lineages were defined as follows: $CD4^+CD3^+CD7^+$ $CD4^+$ T-cells, $CD8a/b^+CD3^+CD7^+$ $CD8^+$ T-cells, $CD7^-CD20/IgM^+$ B-cells, $CD3^+CD7^+TCR\gamma\delta^+$ non-conventional T-cells (NCTs), $CD3^-CD7^+$ innate lymphoid cells (ILCs) including NK-cells and Lin^-cKit^+ HSPCs. All remaining cells were considered myeloid cells. (B) Principal component analysis of the 7 AA^{PRE} and 7 HD bone marrow samples. Each larger dot represents the group mean. Each smaller dot represents a sample. (C) Major immune lineage frequencies in AA^{PRE} and HDs, shown as a percentage of all $CD45^+$ cells in bone marrow. Each black dot represents a sample. Box plots present the median with the interquartile range (IQR), error bars present 1.5*IQR.

Stem cell depletion and high frequencies of $CD16^+$ myeloid cells in AA pre-ATG

Since myeloid, B-cell, $CD4^+$ T-cell and $CD8^+$ T-cell frequencies were significantly different in the bone marrow from AA^{PRE} compared to HDs, we studied each of these lineages at the immune subpopulation level. First, the myeloid cells including HSPCs were selected and analyzed at the four successive levels of the HSNE analysis (Figure 2; Figure S2). In this manner, multiple HSPC and myeloid cell populations could be distinguished based on the expression of defining cell surface markers (Figure 2A, right panels). Twenty phenotypically distinct clusters were identified (Figure 2B), 8 of which were significantly different in AA^{PRE} compared to HDs, 1 had a p-value of 0.053 and 11 clusters did not significantly differ between both groups. Analysis of the 8 significant clusters and cluster 9 showed a strong reduction in all $cKit^{+/dim}$ clusters (cluster #9-11) in AA^{PRE}, confirming HSPC depletion in AA^{PRE} (Figure 2C). Furthermore, we observed a decrease of myeloid cells compatible with $CD123^+$ plasmacytoid dendritic cells (cluster #13), CD163⁺ macrophages (cluster #16), CD11c⁺ conventional dendritic cells (cluster #17) and CD14⁺CD16⁻ classical monocytes (cluster #18) in AA^{PRE}. The most striking observation was a substantial increase in CD16⁺ myeloid cells in AA^{PRE}, which lacked expression of the neutrophil marker CD15 and represented a median of 41% (range 16-83%) of all myeloid cells (Figure S4A-B cluster #14 and 19-20 combined; arrows in Figure 2A). Two CD16⁺ myeloid cell clusters (cluster #19-20) resembling CD14⁻CD16⁺ non-classical and CD14⁺CD16⁺ intermediate monocytes were significantly increased in AA^{PRE} (Figure 2D). In contrast, CD16⁺ myeloid cells only comprised a median of 5% (range 2-19%) of all myeloid cells in HDs (Figure S4A-B).

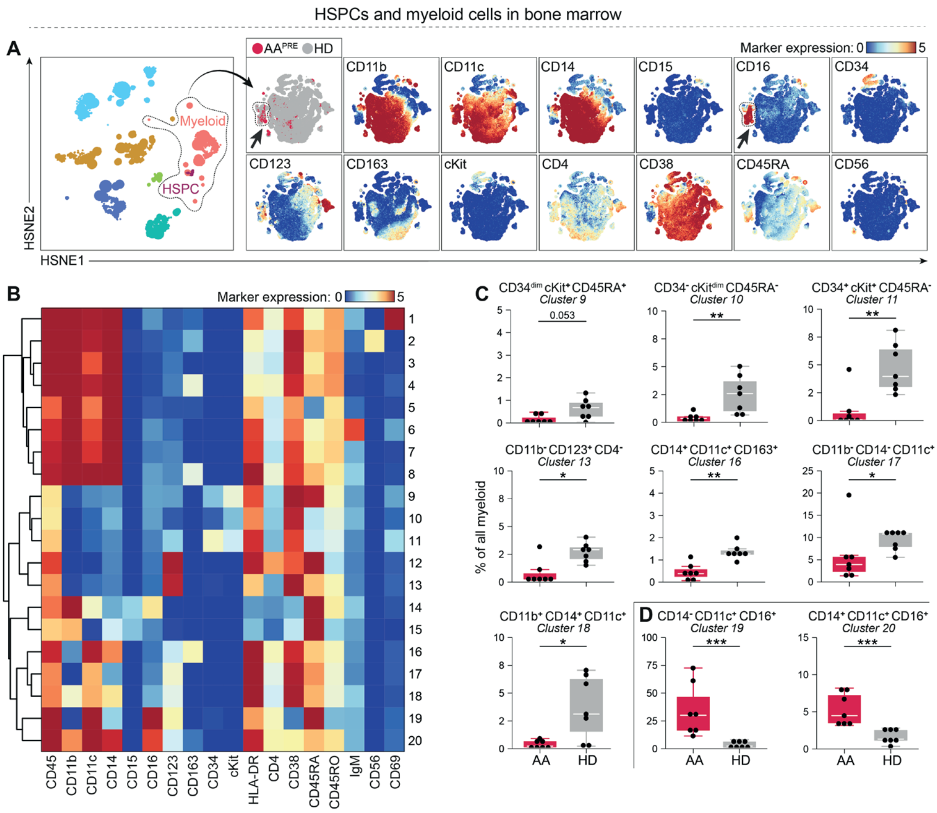

Figure 2. Myeloid cell compartment including HSPCs in bone marrow in AA pre-ATG and HD. Colors indicate major immune lineages (HSPCs, myeloid cells, B-cells, CD4⁺ T-cells, CD8⁺ T-cells, NCT-cells and ILCs), groups (AA^{PRE} in red or HDs in gray) or median arcsinh-transformed marker expression values. (A) HSPCs and myeloid cells isolated from bone marrow of 7 AA^{PRE} and 7 HDs, visualized at level four of a five-level HSNE analysis. $2.4 \cdot 10^5$ landmarks represent $1.3 \cdot 10^6$ cells. The size of each landmark reflects the number of cells represented by the landmark. Arrows indicate CD16⁺ myeloid cells. (B) Heatmap presenting median arcsinh-transformed marker expression values for the 20 clusters identified within the HSPC and myeloid cell compartment. The relationships of similarity between clusters are depicted by the dendrogram. (C) HSPC and myeloid cell clusters reduced in AA^{PRE}. (D) HSPC and myeloid cell clusters increased in AA^{PRE}. Cluster frequencies are presented as a percentage of all HSPCs and myeloid cells in bone marrow from each respective patient or HD. Each black dot represents a sample. Box plots present the median with the interquartile range (IQR), error bars present 1.5*IQR. Only clusters that significantly differed in frequency between AA^{PRE} and HDs are shown.

$CCR6^{++}$ B-cells predominate in AA pre-ATG

Detailed analysis of all B-cells revealed phenotypical heterogeneity within the B-cell compartment (Figure 3A). 20 B-cell clusters were identified (Figure S4C). $CD20^{+}IgM^{-}CD127^{+}$ B-cells (cluster #2) and $CD20^{-}IgM^{-}$ B-cells expressing variable levels of CD127 (cluster #3-4), compatible with a group of early B-cells[19,20], were markedly reduced in AA^{PRE} compared to HDs (Figure 3B). We also observed a decrease in B-cells with absent or low expression of the chemokine receptor CCR6 (Figure 3B, cluster #14 and 17-20). Strikingly, B-cells expressing high levels of CCR6 were strongly increased in AA^{PRE} compared to HDs (Figure 3C, cluster #12-13 and 16). Combined, $CCR6^{++}$ B-cells constituted a median of 64% (range 38-86%) of all B-cells in AA^{PRE} and only a median of 10% (range 1-26%) of all B-cells in HDs (Figure S4C-D, cluster #5, 9, 12-13 and 16 combined). Clusters 12 and 16 co-expressed CD27 in line with previous descriptions of memory B-cells[21-23] (Figure S4C). In contrast, cluster 13 lacked expression of CD27, compatible with a population of immature or mature B-cells[24]. In addition, the $CCR6^{++}$ B-cells expressed different levels of IgM, indicating that these cells were in multiple stages of development.

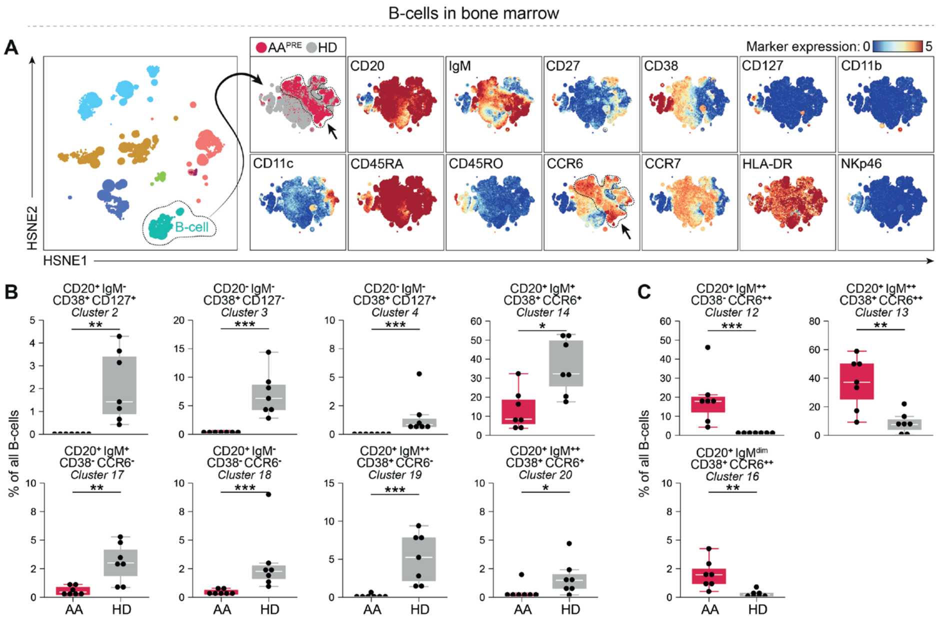

Figure 3. B-cell compartment in bone marrow in AA pre-ATG and HD. Colors indicate major immune lineages (HSPCs, myeloid cells, B-cells, $CD4^{+}$ T-cells, $CD8^{+}$ T-cells, NCT-cells and ILCs), groups (AA^{PRE} in red or HDs in gray) or median arcsinh-transformed marker expression values. (A) B-cells isolated from bone marrow of 7 AA^{PRE} and 7 HDs, visualized at level four of a five-level HSNE analysis. The HSNE depicts $1.6 \cdot 10^{5}$ landmarks for $0.9 \cdot 10^{6}$ B-cells. The size of each landmark reflects the number of cells represented by the landmark. Arrows indicate $CCR6^{++}$ B-cells. (B) B-cell clusters reduced in AA^{PRE}. (C) B-cell clusters increased in AA^{PRE}. Cluster frequencies are presented as a percentage of all B-cells in bone marrow from each respective patient or HD. Each black dot represents a sample. Box plots present the median with the interquartile range (IQR), error bars present 1.5*IQR. Only clusters that significantly differed in frequency between AA^{PRE} and HDs are shown.

Th17-like CCR6$^+$CD4$^+$ T-cells are increased in AA pre-ATG

Hierarchical clustering of all CD4$^+$ T-cells classified 35 phenotypically distinct CD4$^+$ T-cell clusters in different stages of development (Figures S4E-G). No significant differences were observed in naïve (CD45RA$^+$CCR7$^+$) CD4$^+$ T-cell clusters. In contrast, multiple central memory (CM; CD45RO$^+$CCR7$^+$) and effector memory (EM; CD45RO$^+$CCR7$^-$) CD4$^+$ T-cell clusters were significantly reduced in AA^{PRE} (Figure 4A). The most remarkable difference was an increase in CM and EM CD4$^+$ T-cells with a Th17-like phenotype based on the co-expression of CCR6 and/or CD161[25], suggestive of Th17-skewing in AA^{PRE}. Six CCR6$^+$CD4$^+$ T-cell clusters were significantly increased in AA^{PRE} compared to HDs (Figure 4B). Together, the CCR6$^+$CD4$^+$ T-cells represented a median of 11% (range 5-18%) of CD4$^+$ T-cells in AA^{PRE}, compared to a median of 2% (range 2-6%) of CD4$^+$ T-cells in HDs (Figure S4F-G, cluster #13, 16, 18, 20, 22 and 34-35 combined).

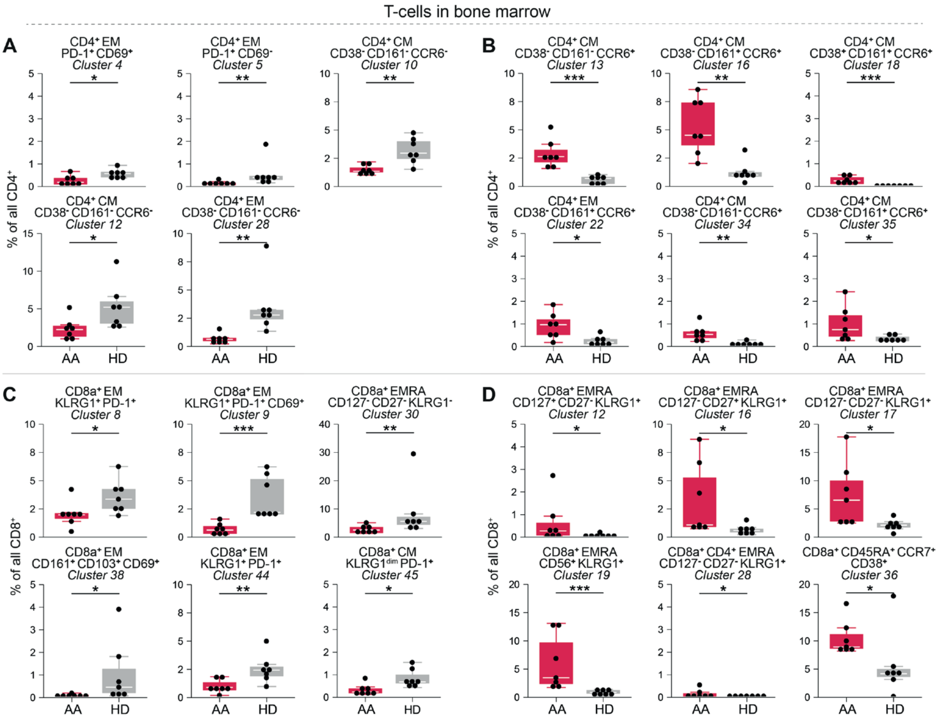

Figure 4. CD4$^+$ T-cell and CD8$^+$ T-cell compartment in bone marrow in AA pre-ATG and HD. Colors indicate groups (AA^{PRE} in red or HDs in gray). (A) CD4$^+$ T-cell clusters reduced in AA^{PRE}. (B) CD4$^+$ T-cell clusters increased in AA^{PRE}. (C) CD8$^+$ T-cell clusters reduced in AA^{PRE}. (D) CD8$^+$ T-cell clusters increased in AA^{PRE}. Cluster frequencies are presented as a percentage of all CD4$^+$ T-cells or CD8$^+$ T-cells in bone marrow from each respective patient or HD. Each black dot represents a sample. Box plots present the median with the interquartile range (IQR), error bars present 1.5*IQR. Only clusters that significantly differed in frequency between AA^{PRE} and HDs are shown.

Increase of KLRG1$^+$ terminally differentiated effector memory CD8$^+$ T-cells in AA pre-ATG

Hierarchical clustering of all CD8$^+$ T-cells identified 45 phenotypically distinct CD8$^+$ T-cell clusters (Figures S4H-J). CM and EM CD8$^+$ T-cells were predominantly reduced in AA^{PRE} (Figure 4C; Figure S4I-J). A cluster of CD8$^+$ T-cells (cluster #36) resembling a population of naïve but activated (CD38$^+$) T-cells was significantly increased in AA^{PRE} (Figure 4D). The most striking observation within the CD8$^+$ T-cell compartment in AA^{PRE} was an increase of EMRA CD8$^+$ T-cells positive for KLRG1 resembling highly differentiated cytotoxic T-cells[26]. These KLRG1$^+$ EMRA CD8$^+$ T-cells constituted a median of 29% (range 15-45%) of all CD8$^+$ T-cells in AA^{PRE}, but only a median of 9% (range 7-33%) of all CD8$^+$ T-cells in the HDs (cluster #10-22, 24-26 and 28-29 combined; Figure S4I-J). Five KLRG1$^+$EMRA CD8$^+$ T-cell clusters (cluster #12, 16-17, 19 and 28) were significantly elevated in AA^{PRE} compared to HDs (Figure 4D).

A disease-specific immune cell network characterizes AA pre-ATG

To capture the relationships across the immune cell clusters that characterize AA^{PRE}, we performed a Spearman's rank correlation analysis on the myeloid, B-cell and T-cell clusters with significant differential presence between AA^{PRE} and HDs. A matrix of Spearman's correlation coefficients visualized two large networks of immune cells (Figure 5A). In line with the analysis of the major immune lineages above, network 1 showed a correlation between CD16$^+$ myeloid cells, CCR6^{++} B-cells, CCR6$^+$ memory CD4$^+$ T-cells, CD45RA$^+$CCR7$^+$CD38$^+$ CD8$^+$ T-cells and KLRG1$^+$EMRA CD8$^+$ T-cells, and was significantly more abundant in AA^{PRE} compared to HDs (median 22% *versus* 5% of CD45$^+$ cells, Figure 5B). In contrast, network 2 was significantly reduced in AA^{PRE} compared to HDs (median 6% *versus* 23% of CD45$^+$ cells). Analysis of paired peripheral blood and bone marrow samples from all 7 AA^{PRE} demonstrated that all subpopulations of network 1 are detectable in peripheral blood (Figure S5).

IST normalizes the immune cell composition in patients with adequate hematological improvement six months post-ATG

Since IST can result in recovery of hematopoiesis, we investigated the effect of IST on the immune cell composition in the bone marrow of 3 AA patients pre- and six months post-ATG. All patients still received ciclosporin and were transfusion-independent six months post-ATG. All patients had improvement of peripheral blood counts and eventually responded to IST, however, only one patient (AA3) showed complete response six months post-ATG (8.3 mmol hemoglobin/L, $149 \cdot 10^9$ platelets/L and $1.8 \cdot 10^9$ neutrophils/L). One patient (AA2) had major partial response six months post-ATG (5.8 mmol hemoglobin/L, $87 \cdot 10^9$ platelets/L and $1.9 \cdot 10^9$ neutrophils/L), while the third patient (AA1) showed minor partial response six months post-ATG (5.4 mmol hemoglobin/L, $18 \cdot 10^9$ platelets/L and $0.3 \cdot 10^9$ neutrophils/L).

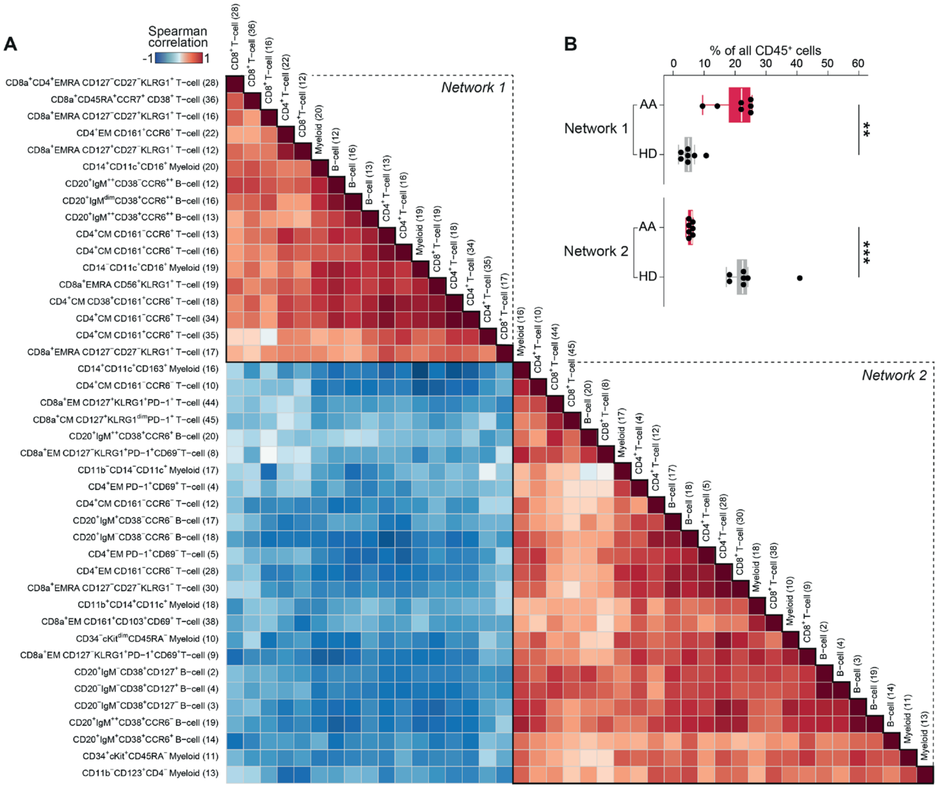

Figure 5. Spearman's rank correlation analysis of differentially present myeloid, B-cell and T-cell clusters in bone marrow in AA pre-IST and HD. (A) Spearman's rank correlation analysis based on the frequencies of all differentially present cell clusters in AA^{PRE} compared to HDs. All AA^{PRE} (n=7) and HDs (n=7) samples were included in the analysis. The strength of the correlations is presented in color (blue to red). The phenotype of each cell cluster is presented left of the correlation matrix. The number of each cell cluster is shown between brackets and corresponds to the cell cluster numbers used in Figures 2 and 3 and Supplemental Figure 3. (B) Total frequency of all cell clusters in networks 1 or 2, expressed as a percentage of all $CD45^+$ cells in bone marrow from each respective patient or HD. Colors indicate groups (AA^{PRE} in red or HDs in gray). Each black dot represents a sample. Box plots present the median with the interquartile range (IQR), error bars present 1.5*IQR.

A total of $3.0 \cdot 10^6$ $CD45^+$ cells (median $0.5 \cdot 10^6$ or $0.3 \cdot 10^6$ cells per AA^{PRE} or AA^{POST}, respectively) were analyzed using a four-level HSNE analysis. At the overview level, the global immune cell composition in AA^{PRE} and AA^{POST} was visualized and all major immune lineages were identified (Figure 6A). HSPCs were not observed, suggesting that the frequency of HSPCs was too low to be detected. Unsupervised PCA presented a clear separation of AA^{PRE} and AA^{POST} (Figure 6B), indicative of a considerable shift in the immune cell composition in the bone marrow six months post-ATG. Analyses at the major immune lineage level demonstrated that myeloid cells were strongly increased or normalized in all AA^{POST} (Figure 6C). In addition, $CD4^+$ T-cells were normalized, while B-cells were still below normal levels in all AA^{POST}. $CD8^+$ T-cells remained high in the patient (AA1) with the lowest blood counts six months post-ATG (Figure 6C).

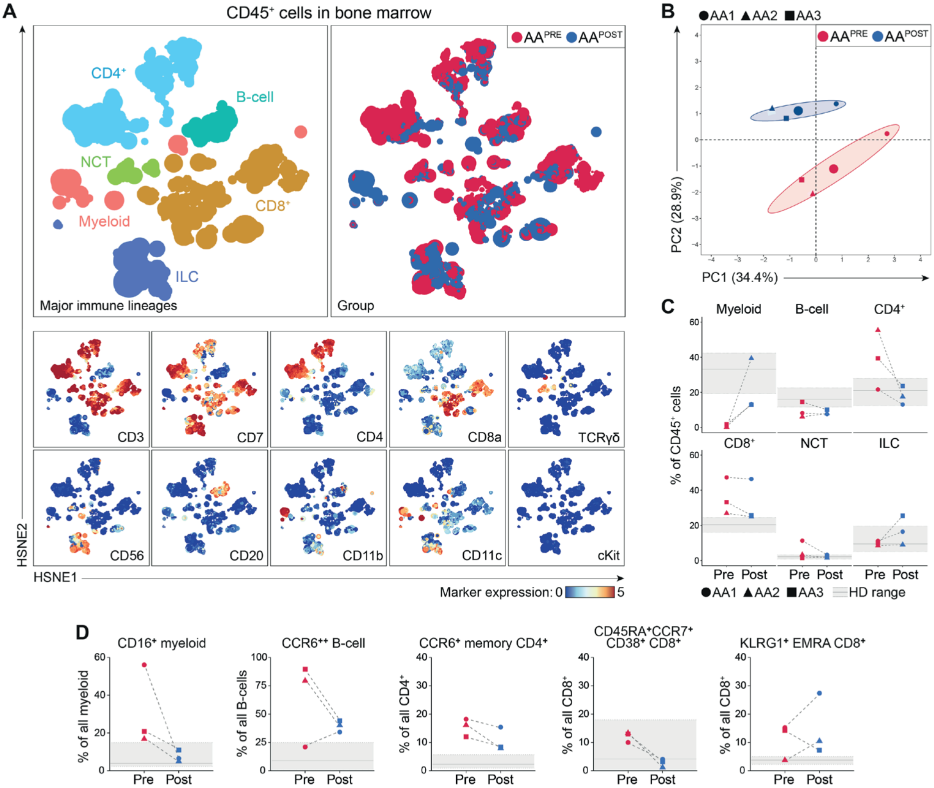

Figure 6. Identification and frequencies of major immune lineages in bone marrow in AA pre- and post-ATG. Colors indicate major immune lineages (myeloid cells, B-cells, $CD4^+$ T-cells, $CD8^+$ T-cells, NCT-cells and ILCs), groups (AA^{PRE} in red and AA^{POST} in blue) or median ArcSinh-transformed marker expression values. (A) Major immune lineages visualized at the overview level of a four-level HSNE analysis with $3.0{\cdot}10^6$ $CD45^+$ cells isolated from paired bone marrow samples collected from 3 AA patients before and six months post-ATG. $1.7{\cdot}10^4$ landmarks represented all $3.0{\cdot}10^6$ $CD45^+$ cells in the analysis. The size of each landmark reflects the number of cells represented by the landmark. (B) Principal component analysis of the 3 AA^{PRE} and 3 AA^{POST} samples. Each larger dot represents the group mean. Each smaller dot represents a sample. (C) Major immune lineage frequencies in the AA^{PRE} and AA^{POST} samples, shown as a percentage of all $CD45^+$ cells in bone marrow from each respective patient or HD. (D) Total pre- and post-ATG frequencies of the $CD16^+$ myeloid cell, $CCR6^{++}$ B-cell, $CCR6^+$ CM or EM $CD4^+$ T-cell, $CD45RA^+CCR7^+CD38^+$ $CD8^+$ T-cell and KLRG1⁺ EMRA $CD8^+$ T-cell clusters representing the immune cell network that was significantly increased in AA^{PRE} compared to HDs. Pre- and post-ATG samples of every AA patient are connected by a dotted line. Minimum and maximum ranges of shaded regions depict the minimum and maximum lineage or subpopulation frequencies in the 7 HDs. Median frequencies in HDs are depicted by a solid gray line. Respective patients are represented by different shapes (AA1 closed circle, AA2 triangle, AA3 square). No P-values are shown because of the small group size.

To analyze the effect of IST on the disease-specific immune cell network identified in AA^{PRE} (network 1), we studied the presence of its corresponding immune cell subtypes in AA^{POST}. Cluster frequencies were compared to frequencies observed in the HDs. Strikingly, this revealed that $CD16^+$ myeloid cell frequencies normalized in all AA^{POST} and $CD45RA^+CCR7^+CD38^+$ $CD8^+$ T-cell frequencies decreased in all AA^{POST} (Figure 6D). $CCR6^{++}$ B-cell, $CCR6^+$ memory $CD4^+$

T-cell and KLRG1$^+$ EMRA frequencies showed a trend towards normalization in the two patients (AA2 and AA3) with complete response or major partial response six months post-ATG. In contrast, these clusters were still frequent or increased in the patient (AA1) with minor partial response six months post-ATG (Figure 6D).

Discussion

The present study provides a comprehensive comparison of the immune landscape in the bone marrow from AA^{PRE} and HDs with the aim to decipher which immune cells may be implicated in the pathogenesis of AA. We demonstrate that the bone marrow from AA^{PRE} harbors a distinct immune cell composition compared to HDs, with significant differences in the myeloid, B-cell, CD4$^+$ T-cell and CD8$^+$ T-cell lineages. Detailed analyses at the immune subpopulation level identified a disease-specific immune cell network of CD16$^+$ myeloid cells, CCR6^{++} B-cells, Th17-like CCR6$^+$CD4$^+$ T-cells, CD45RA$^+$CCR7$^+$CD38$^+$ CD8$^+$ T-cells and KLRG1$^+$ EMRA CD8$^+$ T-cells that distinguishes AA^{PRE} from HDs. This network showed a trend towards normalization in patients with hematological improvement six months post-ATG, which implies a pathogenic role of the network in AA.

To date, cytotoxic T-cells have been the focus of immunophenotyping studies in AA. The present study shows CD4$^+$ and CD8$^+$ T-cell derangements in AA^{PRE}, consistent with the view that AA is mediated by an autologous T-cell response. The identified disease-specific immune cell network featured a group of KLRG1$^+$EMRA CD8$^+$ T-cells, which accords with previous reports on autoimmune disorders[27,28] where KLRG1$^+$CD8$^+$ T-cells accumulate at inflammatory sites. Although CD57 expression was not evaluated in our study, the KLRG1$^+$CD8$^+$ T-cells could resemble previous descriptions of CD57$^+$CD28$^-$ CD8$^+$ T-cells, which commonly express KLRG1[29] and are expanded in peripheral blood [30] in AA where their presence seems to correlate with disease activity[31]. We assume, therefore, that the identified KLRG1$^+$CD8$^+$ T-cells have cytotoxic capacity. The target of this immune response remains presently unknown and would be an interesting topic for future studies.

Within the CD4$^+$ T-cell compartment, we observed increased frequencies of CCR6$^+$ Th17-like cells in the bone marrow of AA^{PRE} compared to HDs. Previous studies postulated a role for Th17 cells in the pathogenesis of AA and identified Th17 cells based on the expression of IL-17[8,32] or CD161[9]. Our data are in line with these studies and add CCR6 as a new marker to delineate Th17 cells in AA. Functionally, Th17 cells may contribute to the immune response in AA through their ability to secrete pro-inflammatory cytokines including IL-17 and IL-21 which can trigger macrophage recruitment and activation.

Interestingly, B-cells are not well characterized in AA, even though B-cell involvement is increasingly recognized in autoimmune disorders. We identified high proportions of CCR6^{++} B-cells that have not been described in AA before but are profoundly increased in autoimmune disorders[33]. Together with the identification of Th17-like CCR6^{+}CD4^{+} T-cells, this presents CCR6 as a potentially important marker in the pathogenesis of AA. CCR6 is a chemokine receptor expressed on various immune cell types and mediates immune cell recruitment to inflammatory sites through CCL20, its sole ligand[34]. Increased levels of CCL20 have been described in the bone marrow in AA[35]. Hence, it is tempting to speculate that the CCR6-CCL20 axis fuels an immune response in AA, as proposed in other autoimmune disorders[36,37], by recruiting pro-inflammatory immune cells to the bone marrow.

Autoimmune responses are generally characterized by an expansion of effector T-cells, rather than an accumulation of polyclonal, antigen-inexperienced naïve T-cells. Therefore, it is surprising that our results point to the importance of a cluster of CD45RA^{+}CCR7^{+}CD38^{+} CD8^{+} T-cells with a naïve phenotype. Since previous work has demonstrated the increased presence of CD95^{+} stem cell-like memory T-cells (T_{SCM}) within the naïve CD8^{+} T-cell compartment in AA[38], we consider the possibility that the CD45RA^{+}CCR7^{+}CD38^{+} CD8^{+} T-cells are CD8^{+} T_{SCM}. T_{SCM} are endowed with an enhanced capacity for self-renewal and control immune responses through their ability to generate memory and effector T-cells[39]. However, because our panel did not include T_{SCM}-specific markers, the precise identity of the CD45RA^{+}CCR7^{+}CD38^{+} CD8^{+} T-cells remains unclear.

The presence of CD16^{+} myeloid cells in the identified immune cell network is striking because AA is characterized by a profound reduction of the myeloid compartment in peripheral blood. Therefore, it would be interesting to determine whether these cells are expanded or are the only myeloid cells left in the bone marrow after immune-mediated destruction in AA. Higher percentages of CD16^{+} macrophages, defined by the expression of CD68 and lower levels of CD14, have been reported in bone marrow in AA, and were suggested to exert bone marrow destructive effects by stimulating effector T-cells through the secretion of TNF-α[40]. We characterized the CD16^{+} myeloid cells in further detail and identified two populations that expressed different levels of CD11b and CD14 and did not express the M2-macrophage marker CD163. Based on this expression profile, these CD16^{+} myeloid cells could represent a population of CD14^{+}CD16^{+} intermediate and CD14^{-}CD16^{+} non-classical monocytes, which can express CD68[20], produce TNF-α[41] and contribute to autoimmune disorders[42,43]. Regarding the function of these cells, one could speculate whether these cells have a direct role in HSPC destruction, e.g. by cytokine secretion, or that they are recruited to clear dead and dying cells, e.g. by antibody-dependent cell-mediated cytotoxicity, and merely reflect a consequence of the immune response.

Altogether, the disease-specific immune cell network identified in the bone marrow from AA^{PRE} is compatible with a state of chronic inflammation. Although this study did not aim to interrogate the functional role of the network, our post-ATG data could indicate a distinct role of $CD16^+$ myeloid cells compared to $CCR6^{++}$ B-cells, Th17-like $CCR6^+CD4^+$ T-cells and $KLRG1^+$EMRA $CD8^+$ T-cells. ATG-based IST can result in the recovery of hematopoiesis, which implies that IST intervenes with the immune response that underlies the pathogenesis of AA. We demonstrate that $CD16^+$ myeloid cells were normalized six months post-ATG, but that $CCR6^{++}$ B-cells, $CCR6^+$ Th17-like $CD4^+$ T-cells and $KLRG1^+$EMRA $CD8^+$ T-cells remained elevated in patients with hematological improvement, despite a trend towards normalization. A possible explanation for the fact that only $CD16^+$ myeloid cells were strongly reduced six months post-ATG could be that these cells are charged with clearing dead and dying cells in the bone marrow in AA, which would explain the decrease in these cells once the initiating immune response has resolved. However, the decrease in $CD16^+$ myeloid cells could also indicate that these cells carry out an effector function in the immune response in AA via cytokine secretion. This would explain the recovery of hematopoiesis after the depletion of $CD16^+$ myeloid cells six months post-ATG. As ciclosporin suppresses B-cell[44] and T-cell development[45], we hypothesize that ciclosporin suppresses the $CCR6^{++}$ B-cells, Th17-like $CCR6^+CD4^+$ T-cells and $KLRG1^+$EMRA $CD8^+$ T-cells that are still elevated six months post-ATG to maintain stable hematopoiesis. The fact that ciclosporin suppression is needed beyond six months could implicate a role for these cells in the initiation of the inflammatory process. Regarding the potential significance of $CCR6^{++}$ B-cells, it is tempting to speculate that hATG-based IST, the preferred first-line treatment in AA, may be more potent at depleting $CCR6^{++}$ B-cells than rATG-based IST and is, therefore, superior in the setting of AA. Based on the potential importance of $CCR6^{++}$ B-cells and $CCR6^+$ Th17-like $CD4^+$ T-cells, our study proposes CCR6 as a new potential therapeutic target. Blockade of CCR6 and disruption of the CCR6-CCL20 interaction have been shown to reduce severity of several autoimmune disorders[46,47]. Multiple reports describe CCR6 blockade therapies targeting pathogenic Th17 T-cells[46,48] and show improvement in diseases such as psoriasis[47] through the inhibition of T-cell recruitment to inflammatory sites, illustrating that CCR6 blockade could be effective in treating T-cell mediated autoimmune disorders. Another report proposes a small molecule inhibitor of CCR6 as a potential therapy for autoimmune disorders through its ability to inhibit CCR6-dependent B-cell migration[49]. Whether anti-CCR6 treatment may be used to control inflammation and symptoms in the active phase of AA could be subject of further studies.

To investigate the clinical applicability of our work, we analyzed peripheral blood for the presence of the disease-specific immune cell network and found that all subpopulations of the immune cell network are detectable in paired peripheral blood and bone marrow samples from AA^{PRE} The fact that the disease-specific immune cell network can be measured in peripheral blood offers possibilities for its clinical use as a marker of disease activity to evaluate the success of IST and possible disease progression.

In summary, we identified a disease-specific immune cell network in the bone marrow from AA^{PRE}. While inflammation-associated immune cells were expected in AA, our approach shows for the first time an association between $CD16^{+}$ myeloid cells, Th17-like cells, $CD45RA^{+}CCR7^{+}CD38^{+}$ $CD8^{+}$ T-cells and $KLRG1^{+}$ EMRA $CD8^{+}$ T-cells and adds $CD16^{+}$ myeloid cells and $CCR6^{++}$ B-cells as a potentially important populations in AA. Successful treatment with IST strongly reduced the levels of $CD16^{+}$ myeloid cells and showed a trend toward normalization of the frequencies of $CCR6^{++}$ B-cells, $CCR6^{+}$ memory $CD4^{+}$ T-cells and $KLRG1^{+}$EMRA $CD8^{+}$ T-cells. The identified network has the potential to be used as a marker for disease activity at diagnosis and during treatment of AA. Together, our study sets the stage for further exploration of the functional relevance and cellular spatial interactions of this immune cell network within the bone marrow microenvironment.

Conflict of interest

The authors declare no competing financial interests.

Author contributions

E.S.P. analyzed results, interpreted the data, made the figures and wrote the manuscript. Y.K-W. performed experiments. V.vU. designed the experimental set-up. J.H.F.F. interpreted the data. F.K. and M.H.M.H. interpreted the data and supervised the project. J.M.L.T. conceptualized the study, recruited patients, interpreted data and supervised the project. All authors critically edited and reviewed the manuscript. All authors approved the final manuscript.

Funding

This work was supported by a research grant from Dioraphte Foundation (grant number 20010406).

Acknowledgements

We thank dr. Tamim Abdelaal of the Department of Radiology of the Leiden University Medical Center for assistance in the data normalization and the network analysis. We acknowledge the Flow Cytometry Core Facility (FCF) of the Leiden University Medical Center for assistance with the generation of the mass cytometry data.

Data availability statement

Mass cytometry data acquired in this study have been deposited to https://flowrepository.org.

Supplemental methods

Mononuclear cell isolation and cryopreservation

Bone marrow mononuclear cells (BMMCs) or peripheral blood mononuclear cells (PBMCs) were isolated from fresh bone marrow aspirates or peripheral blood using Ficoll separation gradient or CPT Cell Preparation Tubes (BD, cat 362780). Subsequently, cells were cryopreserved in liquid nitrogen until further use.

Mass cytometry antibodies

Mass cytometry antibodies and antibody specifications are listed in Supplementary Table 1. The antibodies were either purchased from Standard Biotools or conjugated in-house using Maxpar® X8 Antibody Labeling Kits (Standard Biotools) according to the manufacturer's instructions. After conjugation, antibodies were eluted in 200mL of antibody stabilizer PBS (Candor Biosciences, 131125) containing 0.05% sodium azide and stored at 4°C. All antibodies were previously validated by our group[12-14].

Mass cytometry antibody staining and data acquisition

Cryopreserved BMMC or PBMC samples were measured in six batches. Samples collected from AA^{PRE} and HDs were paired and measured across five batches. BMMC samples taken from AA^{POST} were measured in the sixth batch. A cryopreserved PBMC reference sample was included in batches one and six to account for technical variation. All samples were stained and measured as previously described[14,50]. In brief, cryopreserved BMMCs or PBMCs were thawed, washed, resuspended in 2mL of cell staining buffer (Standard Biotools, cat 201068) and incubated with 1mL of 1:500 Cell-ID™ Intercalator-^{103}Rh 500µM (Standard Biotools, cat 201103A) for 15 minutes at room temperature (RT) to label dead cells. Subsequently, cells were washed, incubated with 5µL of Fc block™ (BD Biosciences, cat 564219) and stained with the 39 metal-isotope tagged antibodies of the mass cytometry panel in a volume of 100µL at RT. After a 45-minute incubation, cells were washed and 1mL of 1:1000 125nM of Cell-ID™ Intercalator-Ir (Standard Biotools, cat 201192A) in fix and perm buffer (Standard Biotools, cat 201067) was added to label nucleated cells. Cells were then stored at 4°C for up to 48 hours. On the day of data acquisition, cells were washed twice in staining buffer and once in MilliQ water. Finally, pelleted cells were resuspended in MilliQ water containing 1:10 EQ Four Element Calibration Beads (Standard Biotools, cat 201078) at a concentration of $0.5\text{-}0.75\cdot10^6$ cells/mL and acquired on the Helios™ mass cytometer (Standard Biotools). At least $0.59\cdot10^6$ (median $0.88\cdot10^6$) events were measured per sample. After measurement, all mass cytometry data were normalized using the EQ bead signal and the reference EQ passport P13H2302.

Analysis of pre- and post-ATG samples

To compare the immune cell composition in bone marrow pre- and post-ATG, paired BMMC samples collected from AA^{PRE} (n=3) and AA^{POST} (n=3) were studied. First, marker distributions across all data files with single, live $CD45^{+}$ cells were aligned using CytoNorm[51] in R version 4.0.5 (R foundation for Statistical Computing) and the PBMC reference samples to correct for a batch effect observed in the data of all post-ATG samples (data not shown). Outputs were checked and confirmed in FlowJo. Next, $3.0{\cdot}10^{6}$ single, live $CD45^{+}$ cells were sample-tagged, hyperbolic arcsinh transformed with a cofactor of 5 and imported into Cytosplore for dimensionality reduction. A four-level HSNE analysis was performed with default perplexity and iterations (30 and 1000, respectively). Three of 39 markers in the mass cytometry panel (HLA-DR, CD20 and CD8a) did not show clear separation between positive and negative populations and thus were not used in the HSNE clustering analysis. Major immune lineages were identified at the overview level of the HSNE analysis by clustering. $CD4^{+}$ T-cells were defined as $CD3^{+}CD7^{+}CD4^{+}$ cells, $CD8^{+}$ T-cells were defined as $CD3^{+}CD7^{+}CD8a/b^{+}$ cells, B-cells were defined as $CD7^{-}CD20/IgM^{+}$ cells, non-conventional T-cells (NCTs) were defined as $CD3^{+}CD7^{+}TCR\gamma\delta^{+}$ cells, innate lymphoid cells (ILCs) including NK-cells were defined as $CD3^{-}CD7^{+}$ cells and HSPCs were defined as $Lin^{-}cKit^{+}$ cells. All remaining cell clusters were considered myeloid cells. Subsequently, each major immune lineage was selected for detailed analysis at the data level of the HSNE analysis using t-distributed stochastic neighbor embedding (tSNE) analyses with up to $0.5{\cdot}10^{6}$ landmarks. Clusters with distinct surface marker expression were identified within each major immune lineage by performing Gaussian mean shift (GMS) clustering at the data level in Cytosplore. Each cluster consisted of at least 1000 cells.

Supplemental tables

Supplemental table 1. 39-marker mass cytometry panel.

Metal	Marker	Clone	Vendor	Dilution
89Y	CD45	HI30	Standard Biotools	1:100
Qdot800	CD14	TuK4	Invitrogen	1:1000
115In	CD15	W6D3	BioLegend	1:50
141Pr	CCR6	G034E3	Standard Biotools	1:100
142Nd	CD34	HIB19	BioLegend	1:100
143Nd	cKit (CD117)	104D2	Standard Biotools	1:100
144Nd	CD69	FN50	Standard Biotools	1:100
145Nd	CD4	RPA-T4	Standard Biotools	1:100
146Nd	CD8a	RPA-T8	Standard Biotools	1:200
147Sm	NKp44 (CD336)	253415	R&D systems	1:40
148Nd	CD16	3G8	Standard Biotools	1:100
149Sm	CD25	2A3	Standard Biotools	1:100
150Nd	IgM	MHM88	BioLegend	1:100
151Eu	CD123	6H6	Standard Biotools	1:100
152Sm	TCRgd	11F2	Standard Biotools	1:50
153Eu	CD7	CD7-6B7	Standard Biotools	1:100
154Sm	CD163	GHI/61	Standard Biotools	1:100
155Gd	CD103	Ber-ACT8	BioLegend	1:100
156Gd	CRTH2 (CD294)	BM16	BioLegend	1:100
158Gd	CD122	TU27	BioLegend	1:50
159Tb	CCR7	G043H7	Standard Biotools	1:100
160Gd	CD5	UCHT2	BioLegend	1:50
161Dy	KLRG1	REA261	MACS	1:50
162Dy	CD11c	Bu15	Standard Biotools	1:200
163Dy	CD20	2H7	BioLegend	1:200
164Dy	CD161	HP-3G10	Standard Biotools	1:100
165Ho	CD127	AO19D5	Standard Biotools	1:200
166Er	CD8b	SIDI8BEE	eBioscience	1:50
167Er	CD27	O323	Standard Biotools	1:100
168Er	HLA-DR	L243	BioLegend	1:300
169Tm	CD45RA	HI100	Standard Biotools	1:100
170Er	CD3	UCHT1	Standard Biotools	1:100
171Yb	CD28	CD28.2	BioLegend	1:100
172Yb	CD38	HIT2	Standard Biotools	1:200
173Yb	CD45RO	UCHL1	BioLegend	1:100
174Yb	NKp46 (CD335)	9E2	BioLegend	1:40
175Lu	PD-1 (CD279)	EH 12.2H7	Standard Biotools	1:100
176Yb	CD56	NCAM16.2	Standard Biotools	1:100
209Bi	CD11b	ICRF44	Standard Biotools	1:100

CCR indicates chemokine receptor; CD: cluster of differentiation; CRTH2: Chemoattractant Receptor-Homologous molecule expressed on T-Helper Type 2 cells; HLA: Human Leukocyte Antigen; Ig: immunoglobulin; KLRG: Killer Cell Lectin-like Receptor; NKp44: Natural Killer Cell P44-related Protein; TCR: T-cell receptor; NKp46: Natural Killer Cell P46-related Protein; PD: Programmed Cell Death Protein.

Supplemental figures

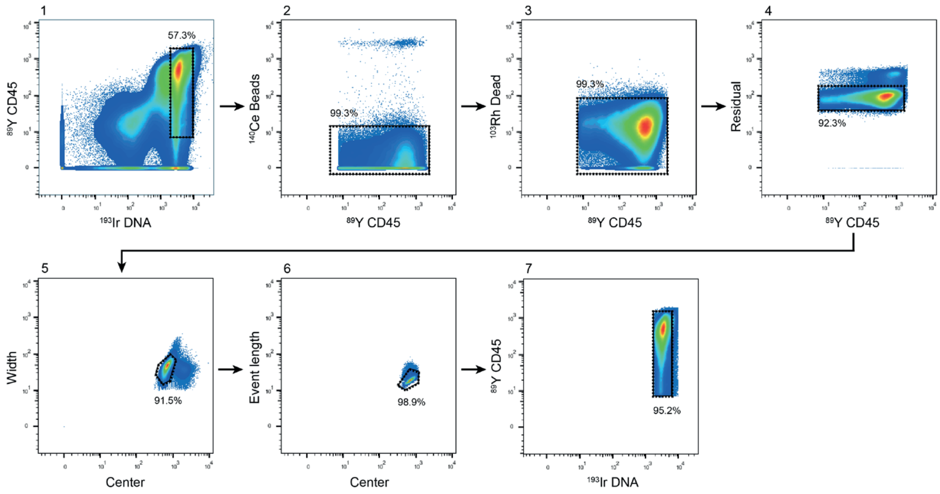

Figure S1. Mass cytometry gating strategy used to identify single, live CD45⁺ cells in bone marrow aspirates. CD45⁺ cells were first gated using CD45 and a DNA marker (panel 1). Subsequently, beads (panel 2), dead cells (panel 3) and doublets and debris (panels 4-6) were eliminated and single, live CD45⁺ cells (panel 7) were exported for analysis. The gating strategy on a representative HD bone marrow aspirate sample is shown.

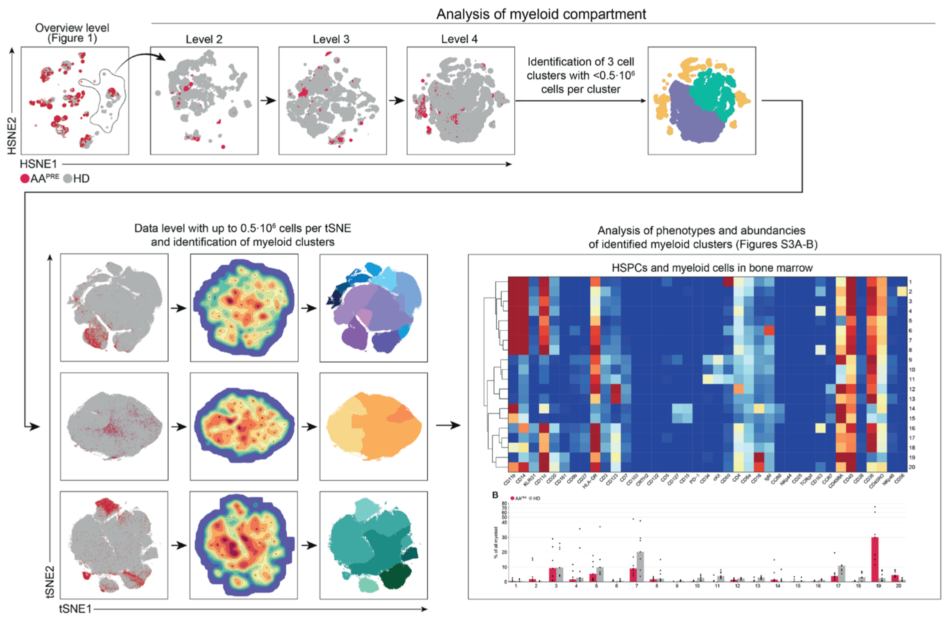

Figure S2. Approach used to analyze each major immune lineage at the immune subset level. HSPCs and myeloid cells are shown as an example. $1.3{\cdot}10^6$ HSPCs and myeloid cells isolated from bone marrow aspirates of 7 AA^{PRE} and 7 HDs were captured at the overview level of the five-level HSNE analysis (Figure 1) and visualized in more detail at levels two ($0.7{\cdot}10^5$ landmarks for $1.3{\cdot}10^6$ cells), three ($4.2{\cdot}10^5$ landmarks for $1.3{\cdot}10^6$ cells) and four ($2.4{\cdot}10^5$ landmarks for $1.3{\cdot}10^6$ cells) of the HSNE analysis. Subsequently, all HSPCs and myeloid cells were divided into three clusters of $\leq 0.5{\cdot}10^6$ cells and studied at the data level. Next, distinct HSPCs and myeloid cell clusters were classified by Gaussian mean shift (GMS) clustering in Cytosplore based on cell densities and differences in marker expression. Finally, marker expression profiles and frequencies of identified clusters were studied in R. Each cluster consisted of at least 1000 cells.

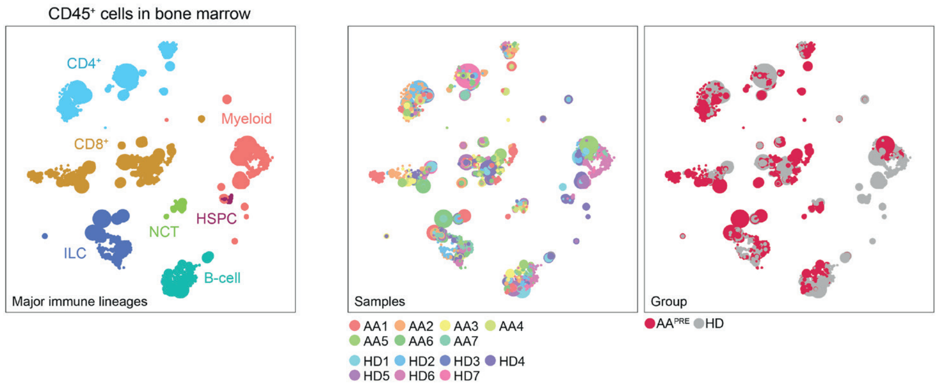

Figure S3. AA^{PRE} and HDs samples visualized at the overview level of the five-level HSNE analysis. Colors indicate major immune lineages (HSPCs, myeloid cells, B-cells, CD4$^+$ T-cells, CD8$^+$ T-cells, NCT-cells and ILCs), samples (7 AA^{PRE} and 7 HDs) or groups (AA^{PRE} in red and HDs in gray). $7.8{\cdot}10^3$ HSNE landmarks represented all $7.7{\cdot}10^6$ CD45$^+$ cells in the analysis. The size of each landmark reflects the number of cells represented by the landmark.

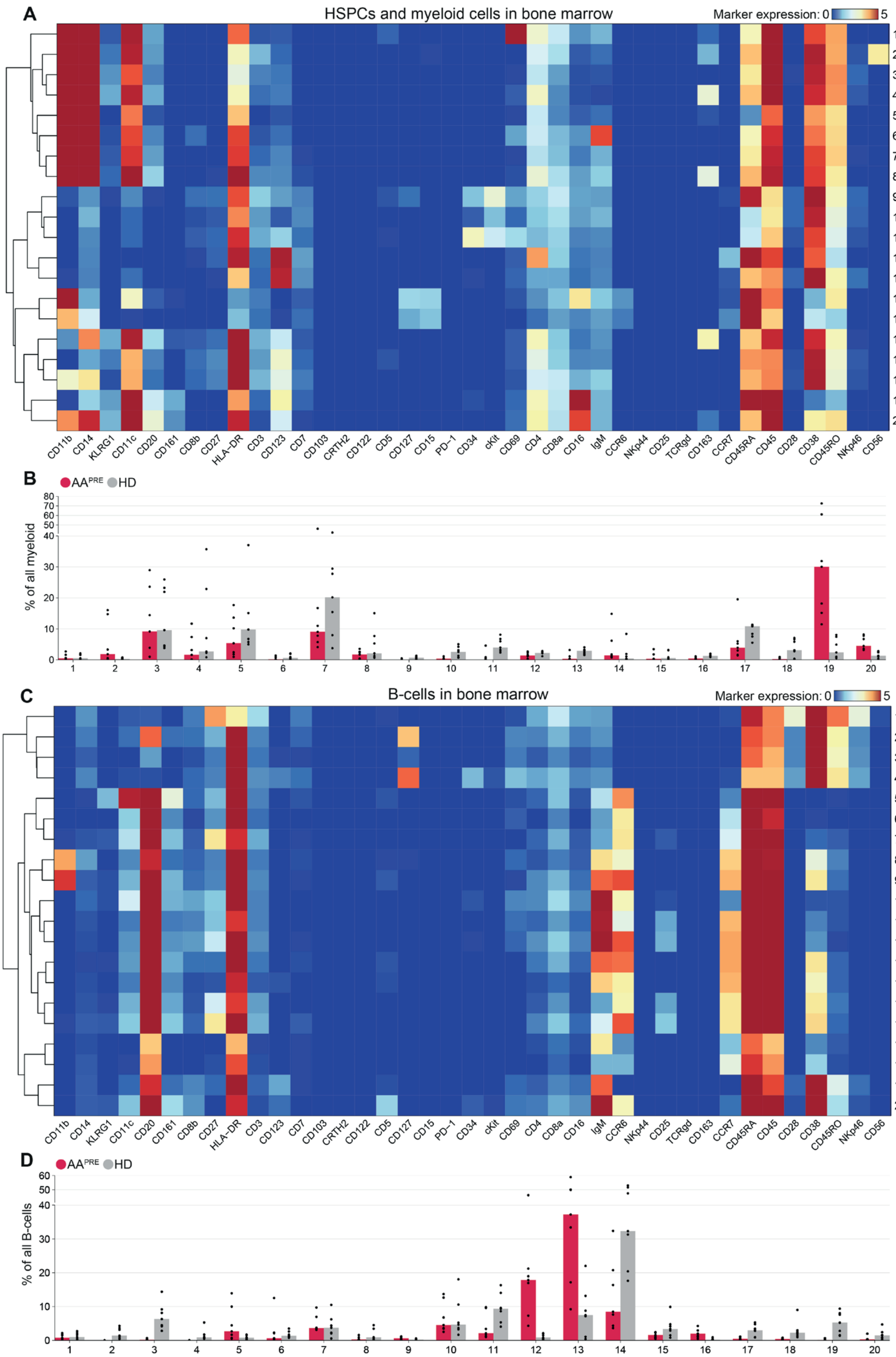
A
HSPCs and myeloid cells in bone marrow
Marker expression: 0 5
CD11b CD14 KLRG1 CD11c CD20 CD161 CD8b CD27 HLA-DR CD3 CD123 CD7 CD103 CRTH2 CD122 CD5 CD127 CD15 PD-1 CD34 cKit CD69 CD4 CD8a CD16 IgM CCR6 NKp44 CD25 TCRgd CD163 CCR7 CD45RA CD45 CD28 CD38 CD45RO NKp46 CD56
B
AA^PRE HD
% of all myeloid
C
B-cells in bone marrow
Marker expression: 0 5
D
AA^PRE HD
% of all B-cells

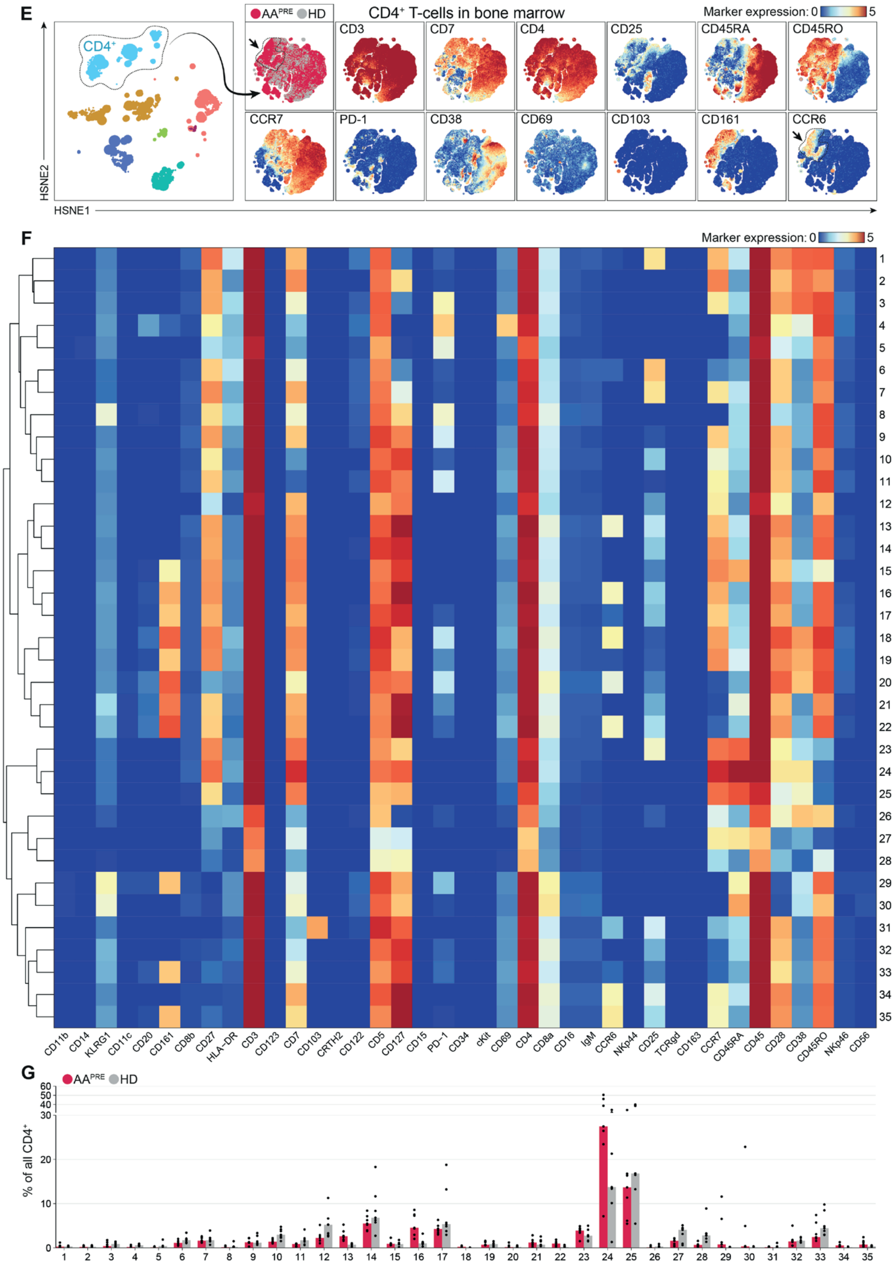
E
CD4+
HSNE1
HSNE2
AAPRE HD
CD4+ T-cells in bone marrow
Marker expression: 0 5
CD3
CD7
CD4
CD25
CD45RA
CD45RO
CCR7
PD-1
CD38
CD69
CD103
CD161
CCR6
F
Marker expression: 0 5
CM
EM
CM
EM
CM
RORA
CM
EM
Naive
EM
Naive
EM
RORA
EM
CM
CD11b CD14 KLRG1 CD11c CD20 CD161 CD8b CD27 HLA-DR CD3 CD123 CD7 CD103 CRTH2 CD122 CD5 CD127 CD15 PD-1 CD34 cKit CD69 CD4 CD8a CD16 IgM CCR6 NKp44 CD25 TCRgd CD163 CCR7 CD45RA CD45 CD28 CD38 CD45RO NKp46 CD56
G
AAPRE HD
% of all CD4+

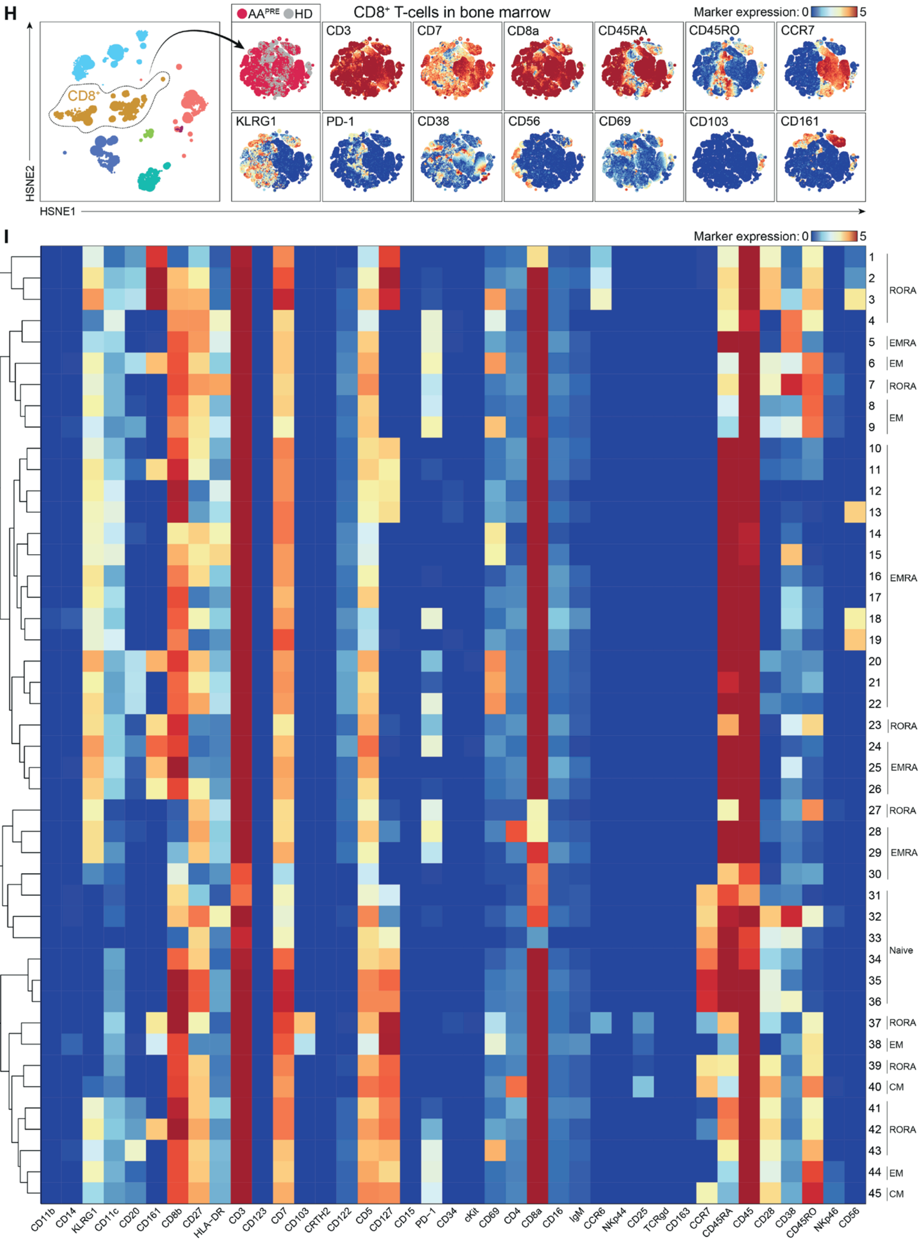
H
AA^PRE HD
CD8⁺ T-cells in bone marrow
Marker expression: 0 5
CD8⁺
CD3
CD7
CD8a
CD45RA
CD45RO
CCR7
KLRG1
PD-1
CD38
CD56
CD69
CD103
CD161
HSNE2
HSNE1
I
Marker expression: 0 5
1
2
3 RORA
4
5 EMRA
6 EM
7 RORA
8
9 EM
10
11
12
13
14
15
16 EMRA
17
18
19
20
21
22
23 RORA
24
25 EMRA
26
27 RORA
28
29 EMRA
30
31
32
33
34 Naive
35
36
37 RORA
38 EM
39 RORA
40 CM
41
42 RORA
43
44 EM
45 CM
CD11b
CD14
KLRG1
CD11c
CD20
CD161
CD8b
CD27
HLA-DR
CD3
CD123
CD7
CD103
CRTH2
CD122
CD5
CD127
CD15
PD-1
CD34
cKit
CD69
CD4
CD8a
CD16
IgM
CCR6
NKp44
CD25
TCRgd
CD163
CCR7
CD45RA
CD45
CD28
CD38
CD45RO
NKp46
CD56

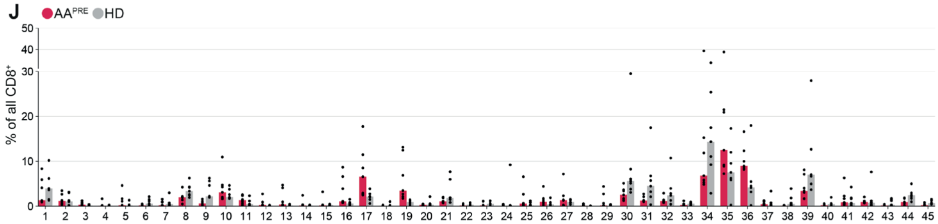

Figure S4. Overview of the myeloid cell, B-cell, CD4⁺ T-cell and CD8⁺ T-cell lineages. Colors indicate major immune lineages (HSPCs, myeloid cells, B-cells, CD4⁺ T-cells, CD8⁺ T-cells, NCT-cells and ILCs), groups (AA^{PRE} or HDs) or median arcsinh-transformed marker expression values. A, C, F, I) Phenotypes of the cell clusters identified within the myeloid, B-cell, CD4⁺ T-cell and CD8⁺ T-cell compartments, respectively. Heatmaps present median arcsinh-transformed marker expression values. The relationships of similarity between cell clusters are depicted by the dendrogram. B, D, G, J) Frequencies of the cell clusters identified within the myeloid cell, B-cell, CD4⁺ T-cell and CD8⁺ T-cell compartments, respectively. Frequencies are presented per group and are shown as a percentage of all cells within a lineage. E, H) CD4⁺ T-cells and CD8⁺ T-cells isolated from bone marrow of 7 AA^{PRE} and 7 HDs, visualized at level four of a five-level HSNE analysis. HSNEs depict $3.4 \cdot 10^5$ landmarks for $1.9 \cdot 10^6$ CD4⁺ T-cells and $3.9 \cdot 10^5$ landmarks for $2.1 \cdot 10^6$ CD8⁺ T-cells. The size of each landmark reflects the number of cells represented by the landmark. Arrows in (E) indicate CCR6⁺ CM and EM CD4⁺ T-cells. RORA: T-cells co-expressing CD45RA and CD45RO.

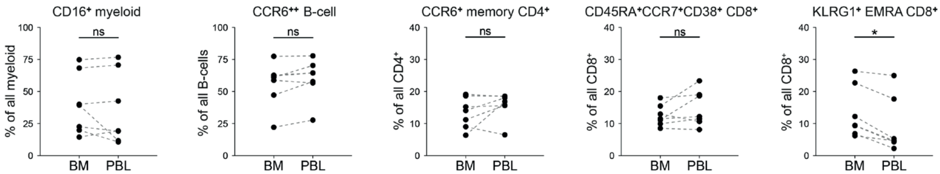

Figure S5. Disease-specific immune cell network can be detected in peripheral blood. Frequencies of the five cell clusters within the identified disease-specific immune cell network, shown in bone marrow and peripheral blood. Paired bone marrow and peripheral blood samples from AA^{PRE} are connected by a dotted line. Bone marrow and peripheral blood samples were compared in an independent analysis to avoid an influence of peripheral blood cells on clustering of bone marrow cells from AA^{PRE} and HDs. Therefore, small differences in cell percentages may be observed between the data presented here and in Figures 2, 3, 4 and 5. The paired bone marrow and peripheral blood samples were compared in a five-level HSNE analysis with default perplexity and iterations (30 and 1000, respectively) and a total of $11.5 \cdot 10^6$ single, live CD45⁺ cells (bone marrow samples from AA^{PRE} and HDs, and peripheral blood samples from AA^{PRE} only). Three of 39 markers in the mass cytometry panel (HLA-DR, CD5 and KLRG1) were not used to generate the HSNE due to small variations in marker distribution between experiments. Major immune lineages were identified at the overview level of the HSNE analysis by clustering based on the phenotypes described in the methods. Subsequently, each major immune lineage was selected for detailed analysis at the data level using tSNE analyses with up to $0.5 \cdot 10^6$ landmarks. Immune cells that matched the phenotypes of the CD16⁺ myeloid cells, CCR6⁺⁺ B-cells, CCR6⁺ memory CD4⁺ T-cells and CD45RA⁺CCR7⁺CD38⁺ CD8⁺ T-cells and KLRG1⁺EMRA CD8⁺ T-cells that were significantly elevated in AA^{PRE} were captured in Cytosplore. Subsequently, their total frequencies were compared between bone marrow and peripheral blood for each individual patient.

References

1. Young NS. Aplastic Anemia. *N Engl J Med*. 2018;379(17):1643-1656.

2. Killick SB, Bown N, Cavenagh J, et al. Guidelines for the diagnosis and management of adult aplastic anaemia. *Br J Haematol*. 2016;172(2):187-207.

3. Tjon JM-L, Zeerleder SS, Groot MRd, et al. Diagnostiek en behandeling verworven aplastische anemie bij volwassenen. *Nederlandse Vereniging voor Hematologie*. 2019.

4. Bacigalupo A, Giammarco S, Sica S. Bone marrow transplantation versus immunosuppressive therapy in patients with acquired severe aplastic anemia. *Int J Hematol*. 2016;104(2):168-174.

5. Halkes CJ, Veelken H, Falkenburg JH. Horse versus rabbit antithymocyte globulin in aplastic anemia. *N Engl J Med*. 2011;365(19):1842-1843; author reply 1843-1844.

6. Scheinberg P, Nunez O, Weinstein B, et al. Horse versus rabbit antithymocyte globulin in acquired aplastic anemia. *N Engl J Med*. 2011;365(5):430-438.

7. Young NS. Pathophysiologic mechanisms in acquired aplastic anemia. *Hematology Am Soc Hematol Educ Program*. 2006:72-77.

8. Kordasti S, Marsh J, Al-Khan S, et al. Functional characterization of CD4+ T cells in aplastic anemia. *Blood*. 2012;119(9):2033-2043.

9. Kordasti S, Costantini B, Seidl T, et al. Deep phenotyping of Tregs identifies an immune signature for idiopathic aplastic anemia and predicts response to treatment. *Blood*. 2016;128(9):1193-1205.

10. Zaimoku Y, Patel BA, Kajigaya S, et al. Deficit of circulating CD19(+) CD24(hi) CD38(hi) regulatory B cells in severe aplastic anaemia. *Br J Haematol*. 2020;190(4):610-617.

11. Bandura DR, Baranov VI, Ornatsky OI, et al. Mass cytometry: technique for real time single cell multitarget immunoassay based on inductively coupled plasma time-of-flight mass spectrometry. *Anal Chem*. 2009;81(16):6813-6822.

12. Li N, van Unen V, Hollt T, et al. Mass cytometry reveals innate lymphoid cell differentiation pathways in the human fetal intestine. *J Exp Med*. 2018;215(5):1383-1396.

13. van der Zwan A, van Unen V, Beyrend G, et al. Visualizing Dynamic Changes at the Maternal-Fetal Interface Throughout Human Pregnancy by Mass Cytometry. *Front Immunol*. 2020;11:571300.

14. van Unen V, Li N, Molendijk I, et al. Mass Cytometry of the Human Mucosal Immune System Identifies Tissue- and Disease-Associated Immune Subsets. *Immunity*. 2016;44(5):1227-1239.

15. Hollt T, Pezzotti N, van Unen V, et al. Cytosplore: Interactive Immune Cell Phenotyping for Large Single-Cell Datasets. *Computer Graphics Forum*. 2016;35(3):171-180.

16. Beyrend G, Stam K, Hollt T, Ossendorp F, Arens R. Cytofast: A workflow for visual and quantitative analysis of flow and mass cytometry data to discover immune signatures and correlations. *Comput Struct Biotechnol J*. 2018;16:435-442.

17. Kassambara A, Mundt F. factoextra: Extract and Visualize the Results of Multivariate Data Analyses. *Version 107*. 2020:CRAN.R-project.org/package=factoextra.

18. Taiyun Wei, Simko V. R package 'corrplot': Visualization of a Correlation Matrix (Version 0.92). 2021.

19. Ryan DH, Nuccie BL, Ritterman I, Liesveld JL, Abboud CN, Insel RA. Expression of interleukin-7 receptor by lineage-negative human bone marrow progenitors with enhanced lymphoid proliferative potential and B-lineage differentiation capacity. *Blood*. 1997;89(3):929-940.

20. Uhlen M, Karlsson MJ, Zhong W, et al. A genome-wide transcriptomic analysis of protein-coding genes in human blood cells. *Science*. 2019;366(6472).

21. Suan D, Krautler NJ, Maag JLV, et al. CCR6 Defines Memory B Cell Precursors in Mouse and Human Germinal Centers, Revealing Light-Zone Location and Predominant Low Antigen Affinity. *Immunity*. 2017;47(6):1142-1153 e1144.

22. Grimsholm O, Piano Mortari E, Davydov AN, et al. The Interplay between CD27(dull) and CD27(bright) B Cells Ensures the Flexibility, Stability, and Resilience of Human B Cell Memory. *Cell Rep*. 2020;30(9):2963-2977 e2966.

23. Agematsu K, Hokibara S, Nagumo H, Komiyama A. CD27: a memory B-cell marker. *Immunol Today*. 2000;21(5):204-206.

24. Sims GP, Ettinger R, Shirota Y, Yarboro CH, Illei GG, Lipsky PE. Identification and characterization of circulating human transitional B cells. *Blood*. 2005;105(11):4390-4398.

25. Annunziato F, Cosmi L, Santarlasci V, et al. Phenotypic and functional features of human Th17 cells. *J Exp Med*. 2007;204(8):1849-1861.

26. Herndler-Brandstetter D, Ishigame H, Shinnakasu R, et al. KLRG1(+) Effector CD8(+) T Cells Lose KLRG1, Differentiate into All Memory T Cell Lineages, and Convey Enhanced Protective Immunity. *Immunity*. 2018;48(4):716-729 e718.

27. Greenberg SA, Pinkus JL, Kong SW, Baecher-Allan C, Amato AA, Dorfman DM. Highly differentiated cytotoxic T cells in inclusion body myositis. *Brain*. 2019;142(9):2590-2604.

28. Li Y, Li B, You Z, et al. Cytotoxic KLRG1 expressing lymphocytes invade portal tracts in primary biliary cholangitis. *J Autoimmun*. 2019;103:102293.

29. Ibegbu CC, Xu YX, Harris W, Maggio D, Miller JD, Kourtis AP. Expression of killer cell lectin-like receptor G1 on antigen-specific human CD8+ T lymphocytes during active, latent, and resolved infection and its relation with CD57. *J Immunol*. 2005;174(10):6088-6094.

30. Kook H, Zeng W, Guibin C, Kirby M, Young NS, Maciejewski JP. Increased cytotoxic T cells with effector phenotype in aplastic anemia and myelodysplasia. *Exp Hematol*. 2001;29(11):1270-1277.

31. Giudice V, Feng X, Lin Z, et al. Deep sequencing and flow cytometric characterization of expanded effector memory CD8(+)CD57(+) T cells frequently reveals T-cell receptor Vbeta oligoclonality and CDR3 homology in acquired aplastic anemia. *Haematologica*. 2018;103(5):759-769.

32. de Latour RP, Visconte V, Takaku T, et al. Th17 immune responses contribute to the pathophysiology of aplastic anemia. *Blood*. 2010;116(20):4175-4184.

33. Lee AYS, Bannan JL, Adams MJ, Korner H. Expression of CCR6 on B cells in systemic lupus erythematosus patients. *Clin Rheumatol*. 2017;36(6):1453-1456.

34. Ito T, Carson WFt, Cavassani KA, Connett JM, Kunkel SL. CCR6 as a mediator of immunity in the lung and gut. *Exp Cell Res*. 2011;317(5):613-619.

35. Ge M, Zheng Y, Li X, et al. Differential expression profile of Th1/Th17/Th2-related chemokines and their receptors in patients with acquired bone marrow failure syndromes. *Hum Immunol*. 2013;74(2):176-180.

36. Meitei HT, Jadhav N, Lal G. CCR6-CCL20 axis as a therapeutic target for autoimmune diseases. *Autoimmun Rev*. 2021;20(7):102846.

37. Ruth JH, Shahrara S, Park CC, et al. Role of macrophage inflammatory protein-3alpha and its ligand CCR6 in rheumatoid arthritis. *Lab Invest*. 2003;83(4):579-588.

38. Hosokawa K, Muranski P, Feng X, et al. Memory Stem T Cells in Autoimmune Disease: High Frequency of Circulating CD8+ Memory Stem Cells in Acquired Aplastic Anemia. *J Immunol*. 2016;196(4):1568-1578.

39. Gattinoni L, Lugli E, Ji Y, et al. A human memory T cell subset with stem cell-like properties. *Nat Med*. 2011;17(10):1290-1297.

40. Sun W, Wu Z, Lin Z, et al. Macrophage TNF-alpha licenses donor T cells in murine bone marrow failure and can be implicated in human aplastic anemia. *Blood*. 2018;132(26):2730-2743.

41. Mukherjee R, Kanti Barman P, Kumar Thatoi P, Tripathy R, Kumar Das B, Ravindran B. Non-Classical monocytes display inflammatory features: Validation in Sepsis and Systemic Lupus Erythematous. *Sci Rep*. 2015;5:13886.

42. Rossol M, Kraus S, Pierer M, Baerwald C, Wagner U. The CD14(bright) CD16+ monocyte subset is expanded in rheumatoid arthritis and promotes expansion of the Th17 cell population. *Arthritis Rheum*. 2012;64(3):671-677.

43. Narasimhan PB, Marcovecchio P, Hamers AAJ, Hedrick CC. Nonclassical Monocytes in Health and Disease. *Annu Rev Immunol*. 2019;37:439-456.

44. Hannam-Harris AC, Taylor DS, Nowell PC. Cyclosporin A directly inhibits human B-cell proliferation by more than a single mechanism. *J Leukoc Biol*. 1985;38(2):231-239.

45. Jenkins MK, Schwartz RH, Pardoll DM. Effects of cyclosporine A on T cell development and clonal deletion. *Science*. 1988;241(4873):1655-1658.

46. Bouma G, Zamuner S, Hicks K, et al. CCL20 neutralization by a monoclonal antibody in healthy subjects selectively inhibits recruitment of CCR6(+) cells in an experimental suction blister. *Br J Clin Pharmacol*. 2017;83(9):1976-1990.

47. Getschman AE, Imai Y, Larsen O, et al. Protein engineering of the chemokine CCL20 prevents psoriasiform dermatitis in an IL-23-dependent murine model. *Proc Natl Acad Sci U S A*. 2017;114(47):12460-12465.

48. Robert R, Juglair L, Lim EX, et al. A fully humanized IgG-like bispecific antibody for effective dual targeting of CXCR3 and CCR6. *PLoS One*. 2017;12(9):e0184278.

49. Tawaraishi T, Sakauchi N, Hidaka K, et al. Identification of a novel series of potent and selective CCR6 inhibitors as biological probes. *Bioorg Med Chem Lett*. 2018;28(18):3067-3072.

50. Bendall SC, Simonds EF, Qiu P, et al. Single-cell mass cytometry of differential immune and drug responses across a human hematopoietic continuum. *Science*. 2011;332(6030):687-696.

51. Van Gassen S, Gaudilliere B, Angst MS, Saeys Y, Aghaeepour N. CytoNorm: A Normalization Algorithm for Cytometry Data. *Cytometry A*. 2020;97(3):268-278.